

A NUMERICAL STUDY OF THE RELEASE AND DISPERSION OF A BUOYANT GAS IN PARTIALLY CONFINED SPACES

K. Prasad¹, W. M. Pitts and J. C. Yang

1. Abstract

Development of the hydrogen economy will require a better understanding of the potential for fires and explosions associated with the unintended release of hydrogen within a structure. The ability to predict the mixing and dispersion behavior of hydrogen, when accidentally released in a partially confined space (e.g. hydrogen leak from automobiles parked in a residential garage) is critical to the safe use of hydrogen products. Hydrogen release and dispersion in a garage can be simulated using computational fluid dynamic (CFD) tools. However, CFD software needs to be validated with experimental data before it can be used reliably for development of codes and standards appropriate for hydrogen fire safety. This paper assesses the capability of a CFD software package to simulate the mixing and dispersion behavior of highly buoyant gases in a partially confined geometry. Simulation results accurately captured the overall trend measured in experiments conducted in a reduced scale enclosure with idealized leaks. The difference between experimentally measured peak concentrations and numerical simulation results, averaged over various heights was 2.3%. Sensitivity of the computed results on various model parameters was determined and is reported in this paper. Results indicate that the size of the leak has a small effect on the predicted concentrations, but the location of the leaks in the garage has a very significant effect on the computed results. This result has important implications on future modeling efforts as well as codes and standards related to hydrogen fire safety.

2. Introduction

Substantial efforts are being directed towards the development of hydrogen-fueled automobiles as an approach for reducing the amount of carbon dioxide generated by transportation systems [1]. The physical and chemical properties of hydrogen are sufficiently different from currently employed hydrocarbon fuels that careful analysis is required to ensure the safety of the new systems. Hydrogen is highly buoyant in air and diffuses rapidly. Therefore its mixing, dispersion (exchange between enclosure and the ambient environment) and burning behavior are very different than those of hydrocarbon fuels. Since a large fraction of a hydrogen-fueled automobile fleet is likely to be kept in existing residential garages, it is important to be able to predict the mixing behavior and dispersion of hydrogen in a garage (partially confined space) following an accidental release [2] of hydrogen.

¹ Corresponding Author: Research Engineer, Fire Research Division, National Institute of Standards and Technology, Gaithersburg, MD 20899, email : kprasad@nist.gov

The dispersion, mixing and combustion of hydrogen in large enclosures has been studied extensively in the literature. Swain et al. [3] have developed a hydrogen risk assessment method (HRAM) to establish the requirements for venting in buildings that contain hydrogen-fueled equipment, using a four step process. In the first step of their proposed methodology, the accident scenario should be constructed with helium released at the expected hydrogen leakage rate. Helium concentrations versus time should be measured at various locations. Secondly, CFD simulations should be performed of the accident scenario (using helium) and the model should be validated with experimental data. Thirdly, the CFD model should be used to predict the behavior of hydrogen (instead of helium) and finally, the risk from the spatial and temporal distribution of hydrogen can be determined. Experiments and numerical simulations were performed in various geometric configurations (hallway, vertical vent) to show that the methodology was suitable for assessing the risk from an accident scenario. Swain et al. [4] have also developed simple rules for assessing the risk from leaks in enclosed spaces as well as in un-enclosed spaces. They concluded that for release into partially enclosed spaces (garage geometry), CFD models should be used to predict the distribution and concentration of hydrogen gas as a first step towards determining the risk associated with the specific leak scenario.

The short and long term mixing and distribution of hydrogen releases in confined spaces was investigated as an internal project of HYSAFE [5]. The experiment consisted of 1 g/s vertical release of hydrogen for 240 s from an orifice of 20 mm diameters into a rectangular room of dimensions 3.78 m x 7.2 m x 2.88 m in width, length and height respectively. Constant pressure conditions inside the compartment (constructed in a rock cave) were assured by the presence of two small openings at the front side of the room close to the floor. Concentration time histories were measured at various locations during the release phase and the subsequent dispersion phase. An inter-comparison exercise [6] was performed with 10 different CFD codes and 8 different turbulence models to predict the short term and the long term mixing behavior. Large variations [6], [7], [8], [9] in predicted results were reported due to differences in turbulence models and numerical accuracy of the various CFD schemes. Simulation results were found to under-predict the experimental data during the dispersion phase.

CFD software has been used extensively in the past by the fluid dynamics and combustion community to study hydrogen leakage and burning in complex geometries [3], [6], [7], [10]-[14]. The NIST Fire Dynamics Simulator (FDS) [15], [16] is one such CFD package that has been used traditionally by the fire protection community to simulate fires in large buildings and for forensic analysis, and can be used effectively for studying hydrogen release and dispersion in a garage [6], [7]. However, FDS needs to be validated with experimental data before it can be used reliably for support and development of codes and standards appropriate for hydrogen fire safety.

Swain and Shriber [10] have compared FLUENT calculations for a gas cloud formation for four different fuels (Hydrogen, Natural Gas, Liquefied Petroleum Gas and Gasoline) following an accidental release (hydrogen leakage was approximately 1000 L/h) with experimental data obtained in a residential garage (2.52 m x 6.59 m x 2.74 m). The air changes per hour (ACH) for the garage were 0.2 or 2.9. Their work provided a basis for predicting the volume of combustible (flammable) gases in enclosed spaces. High pressure leaks of hydrogen ignited at the source has been studied by Schefer and Houf [11] by utilizing turbulent jet flame data. They established a framework for scaling and similarity of the flames over a range of length scales, and the data was used to quantify the larger-scale flames of interest to safety standards. Radiative characteristics of large-scale hydrogen jet flames were compared with experimental and theoretical results for laboratory scale flames [12]. Their work has helped in identifying future research needs for hydrogen safety codes and standards.

In order to validate FDS, a series of experiments have been performed at NIST in which helium was released into a ¼-scale two-car residential garage. Time-resolved measurements of helium volume fractions were made at multiple heights in the model garage during the releases and dispersion phase. FDS simulations of the experimental setup were conducted to accurately resolve the entrainment into the buoyant plume and the leakage through the enclosure openings. Sensitivity studies were conducted to understand the effect of orifice diameter, inlet jet velocity, location and size of the vents, mesh density and other model parameters on the predicted concentrations. This paper will briefly discuss the experiments conducted in the reduced scale partially enclosed geometry, followed by a detailed description of the numerical simulations that have been performed to validate the models, including changes that have been made to the FDS software, sensitivity studies and comparison of the results with available data.

3. Experiments in reduced scale garage geometry

A series of reduced scale experiments [17] were conducted to characterize the mixing and dispersion of helium in a reduced scale garage and to develop a database with which to validate CFD software. An approximately quarter scale two-car residential garage (representative dimension of full scale garages are 6.1 m x 6.1 m x 3.05 m) with interior dimensions of 1.5 m x 1.5 m x 0.745 m was constructed with 1.25 cm thick plexiglas (Figure 1). The box was formed by gluing five sections to form an enclosure with an open wall. Thin sections of plexiglas were placed around the opening to act as a flange. The front wall was sealed to the flange with a greased gasket and held in place by clamps. Due to safety concerns, helium was used as a surrogate for hydrogen. A Fisher burner² was used to release the helium into the compartment. Note that the current set of experiments and simulations (described later) do not involve any burning,

² Certain commercial equipment, instruments, or materials are identified in this document. Such identification does not imply recommendation of endorsement by the National Institute of Standards and Technology, nor does it imply that the products identified are necessarily the best available for the purpose.

however, the term burner is used in this paper to indicate a device through which helium was released into the compartment. The burner was 207 mm tall and the exit diameter was 36 mm (cross-sectional area 10.17 cm²). The burner was expected to produce a fairly uniform room temperature (21 °C) flow at exit. No direct measurements were made on the velocity field at the burner exit or the temperature of the gas leaving the burner. Helium flow through the burner was controlled through a mass flow controller. The specified flow rate for 1 hour and 4 hour releases were 14.95 L/min and 3.74 L/min, respectively (flow rate was scaled to represent the emptying of a 5 kg of hydrogen fuel tank in 1 or 4 hours). Uncertainty in the measurement of the mass flow rate was 1% [17].

A typical garage is not air tight and may contain several small leaks especially concentrated around the garage door and windows. Idealized leaks were chosen to have areas that provide minimum ventilation requirements for residential garages, of 3 ACH with pressure differential of 4 Pa [19]. The leaks consisted of either a single 2.4 cm square opening with a cross-sectional area of 5.76 cm² in the center of one face (flow coefficient of 1.0), or two equal openings (each opening was 2.15 cm square with a cross-section area of 4.62 cm²) centered horizontally at the top and bottom of the front face (flow coefficient of 0.66). Note that the flow coefficient values were used only to design the experiment and not in the numerical simulations. Time-resolved helium volume fractions were measured at seven heights, at one horizontal location (40.5 cm from side and 35.5 cm from front) within the compartment. The vertical location of each sensor (height above the floor) is indicated in Table 1. Results for “Sensor 1” (located furthest from the ceiling at a height of 0.093 m above the floor) and “Sensor 7” (close to the ceiling at a height of 0.65 m above the floor) are discussed extensively in this paper. Each sensor measured the helium concentration during the release phase as well as the subsequent mixing and dispersion phase, until a point was reached when the concentration of the gas was close to the ambient value. Uncertainty in measuring helium concentration was 1% [17]. All the sensor data was recorded and analyzed through a computerized data acquisition system. Limited testing indicated that horizontal variation in volume fraction at the measured heights was small.

4. Numerical Modeling of Reduced Scale Experiments

The reduced scale experiments described above were simulated using the NIST Fire Dynamics Simulator (FDS) [15], [16]. FDS is a CFD code that was explicitly developed for the purpose of computing fire driven flows. In this software, a form of the Navier-Stokes equations appropriate for low-speed, chemically reacting fluid flow are solved. The FDS solver is limited to low Mach number flows and uses a large-eddy sub-model for turbulence modeling in large-scale simulations. The equations describing the conservation of mass, momentum and energy are discretized on a rectilinear grid and second order accurate finite difference approximation of the equations were updated in time.

Numerical simulations of the experimental setup (discussed in the previous section) involving helium mixing and dispersion in partially enclosed reduced

scale geometry were preceded by a large number of exploratory studies on a number of different geometric configurations, to simulate experiments that have been conducted by various researchers all over the world using FDS. Preliminary coarse grid simulations were performed for hydrogen release in a vertical chimney configuration, hallways and single car garages with a single vent in the garage door and the results were compared with published data [3], [4]. This was followed by a numerical model of an experiment conducted at INERIS [5], [6] to study the release of small amounts of hydrogen in a confined space. The experimental setup consisted of a 1 g/s vertical hydrogen release for 240 s from an orifice of 20 mm diameter in a rectangular room (garage) of dimensions 3.78 m x 7.2 m x 2.88 m. Two small openings (50 mm diameter) at the front of the room, close to the floor, assured constant pressure conditions. Hydrogen concentrations were measured as a function of time during both the release phase (240 s) and the subsequent diffusion phase (5160 s) at various heights in the garage. FDS simulation results [17] were compared with experimental data and results from other CFD models. The comparison of the data indicated that the short term mixing behavior (<500 s) was predicted accurately, but the long term response (> 500 s) at some sensors was under-predicted by the simulations [17]. Calculations were also performed to simulate the fan overpressure test in the quarter scale two-car garage. The predicted results on volume flow rate as a function of pressure rise in the compartment were found to compare favorably with measured experimental data. Although the results of these exploratory calculations have not been discussed in this paper in detail, the success in predicting the behavior for hydrogen or helium releases in various geometric configurations provide confidence that FDS can be used to accurately predict the mixing and dispersion of buoyant gases in partially enclosed spaces.

We next describe a detailed numerical study that was performed to simulate the experiment (described in the previous section) on helium release in a reduced scale two-car garage, including comparison with available data and the sensitivity of the results to input parameters. Table 2 summarizes the burner location, release point, leak configuration, leak location and duration of release for the four experiments (Cases A, B, C and D) that have been simulated in this paper. Three burner locations were employed - burner in the center of the compartment resting on the floor (Case A and Case C), burner in the rear of the compartment resting on the floor (Case B), and burner in the center of the compartment and release point close to the ceiling (Case D). The leaks from the compartment were discussed in the previous section and consisted of one hole in the center (Case A, B and D) or two holes at the top and bottom (Case C). The duration of the release was 1 hour (Case A, B and C) or 4 hours (Case D).

Simulation Results and Discussions

Figure 2 shows a Smokeview [20] image of the computational domain used for simulating the experimental setup (Case A). The shaded domain had properties of

plexiglas and dimensions of 1.5 m x 1.5 m x 0.75 m. Hydrogen or helium gas was released through a burner (red color) located in the center of the plexiglas compartment, with a square cross-section (3.13 cm x 3.12 cm) and the area at burner exit was 9.76 cm². The mass flux specified at the burner exit was 0.0422 kg/m²/s, corresponding to an experimentally measured value of 14.95 L/min (the volume flow rate was scaled to simulate the release of 5 kg of hydrogen in 1 hour). The front wall of the compartment has a hole (2.34 cm x 2.32 cm) in the center with a cross-sectional area of 5.43 cm², representing an idealized leak (Figure 2). The computational domain was extended 0.5 m beyond the front wall and open flow boundary conditions were imposed on all the external boundaries in this extended domain. The principal reason for extending the domain was to apply the boundary conditions as far as feasible from the hole and to compute the convective / diffusive flow through the hole as a solution to the governing equations. A 48 x 64 x 64 cartesian mesh was used for the simulations. The grid was concentrated in the region around the burner with minimum grid spacing in the horizontal direction of 7.8 mm, while the grid was uniform in the vertical direction with grid spacing of 11.6 mm. Simulation results presented in Figure 3- Figure 7 are for helium release over a one hour period followed by a mixing and dispersion phase tracked for an additional one hour period (Case A).

Figure 3 shows helium volume fraction on a plane passing through the middle of the computational domain cutting through the burner as well as the hole in the front wall, at 1800 s after the release of helium. The density contours (kg/m³) have been plotted in Figure 4, while the velocity field in the plume region has been shown in Figure 5. Assuming a characteristic length equal to the burner diameter, we obtain a flow Reynolds number of approximately 70 indicating that the flow field is quite laminar (exit velocity was approximately 25 cm/s). The Froude number was found to be 0.46 indicating that the flow field is buoyancy dominated with entrainment into a helium plume, as indicated by the velocity vectors shown in Figure 5. As helium was released from the burner, the buoyant plume quickly rose up to the ceiling and spread horizontally. Air was pushed out through the hole in the front wall, as helium concentration builds up close to the ceiling. Helium also diffused downward and as a result the sensors located close to the floor showed an increase in the helium concentration. Results at 1800 s after the start of the release of helium indicate a very low density (0.7 kg/m³) plume, consisting of helium and entrained air, rising to the ceiling and a stratification of highly concentrated helium close to the ceiling and low concentrations close to the floor. Results indicate that the helium volume fraction variation in the horizontal direction was relatively small, in the region far away from the plume. Note that the domain outside the compartment consisted of pure air (density of 1.2 kg/m³). Velocity vectors show helium flowing out through the hole, rising quickly and flowing through the top of the extended domain. Magnitudes of the velocity vectors inside the compartment away from the plume region and the hole were relatively small. At 3600 s (results now shown), it was observed that the density of gas at the ceiling was very low (0.7 kg/m³) and that a significant quantity of helium had diffused towards the floor. Following the

release phase, the density in the entire compartment became quite uniform, based on the data for 5400 s and 7200 s (results not shown).

Figure 6 shows the mass flow rate (integrated value over the entire cross-section) through the burner (black curve) and through the hole (red curve) as a function of time. The helium flow rate through the burner was set at 4.1×10^{-5} kg/s, corresponding to an experimentally measured volume flow rate of 14.95 L/min. The integrated flow rate through the hole was very high initially, since the gas leaving the hole consisted of pure air. However, as more helium mixed and diffused into the air, the gas leaving through the hole had a lower density (mixture of helium and air) and this density became smaller over time (as seen from Figure 3 and Figure 4). When the helium flow through the burner was stopped after one hour, there was an abrupt change in the mass flow rate through the hole. Beyond this stage the dynamics of the flow through the hole was very complex, since it involved air diffusing into the compartment and helium leaving the compartment. As air entered the compartment it was immediately pushed down towards the floor, while the helium that leaked out through the compartment rose upward due to buoyancy. Both of these effects are captured in our simulations. The integrated mass flow rate through the hole was not smooth during the dispersion phase, because of an oscillating flow (gurgling flow) through the hole and the limited spatial resolution of the flow field through the hole.

Flow induced pressure perturbations (gauge pressure) at three heights above the floor (0.74 m, 0.375 m and 0.01 m) are plotted in Figure 7 as a function of time. These results indicate that the helium plume creates a stratification of the flow field which results in positive flow induced pressure perturbations close to the ceiling and negative perturbations close to the floor. During the release phase, the magnitude of the perturbations increased with time and then reduced gradually during the dispersion phase. As expected, the neutral plane was located at the height of the hole. The pressure perturbations have a significant effect on the dynamics of the flow through the hole, especially during the dispersion phase.

Detailed comparison with experimental data and accuracy of the predicted results

In this section, detailed comparison between experimental data and numerical predictions is discussed for the four cases shown in Table 2, along with the relative accuracy of the computed results. Comparison of experimentally measured helium concentrations (symbols) with predicted values (lines) at seven sensor locations for Case A are shown in Figure 8. Sensor 7 (green) located closest to the ceiling shows a peak volume fraction of approximately 0.47 at the one hour mark, when the helium flow through the burner was stopped. Sensor 4-6 also peak at the one hour mark (as in the experiment data). Sensors 1-3 indicate a concentration profile that continues to rise even after the one hour mark, due to diffusion of helium from the top of the compartment towards the floor. Note that the vertical location of sensors 1-3 was below the hole in the front wall of the compartment. Sensor 1 (orange) showed a peak volume fraction of 0.39. Table 3

lists the relative difference between the numerical simulation results and the experimental data at the point when the helium flow through the burner was stopped, as a percentage of the experimental data for all the sensors. The percentage accuracy averaged over all the sensors, for each case is also computed. Numerical simulation results for Case A under-predict the experimental data at all heights, however the average difference between numerical predictions and experimental data was less than 3.3%.

Figure 9 shows comparison between experimentally measured helium concentrations (symbols) and numerically predicted values (lines) for Case B, where helium was released for one hour through a burner located in the rear of the compartment close to the floor, while the leak consisted of a single hole located in the center of the front wall. The color coding used for the various sensors is similar to that used in Figure 8. Numerical simulations accurately predict the measured trend for all the sensors during the release phase as well as the dispersion phase. The difference between numerical predictions and experimental data expressed as a percentage of the experimental value, and averaged over all the sensors was 2.2 %. Comparison of numerical and experimental data for the case of helium release through a nozzle located in the center of the compartment close to the floor, while the leak consisted of two holes, located at the top and bottom of the front wall of the compartment is shown in Figure 10 (Case C) and the average accuracy relative to the experimental data was 4.6 %. Figure 11 shows a similar plot for the case of a four hour release of helium through a burner located in the center of the compartment close to the ceiling, while the leak consisted of a single hole in the center of the front wall (Case D) with average accuracy of -0.9%. The difference between the experimentally measured peak concentrations and numerical simulation results, averaged over all the sensors and the various cases studied in this paper was found to be 2.3% (Table 3).

Parametric Sensitivity Studies

A series of sensitivity studies were conducted over the input parameters (such as mass flux through the burner, size of the burner, size of the leaks) as well as numerical parameters (such as Smagorinsky constants, Schmidt number etc) to determine the effect of the various parameters on the predicted helium concentration. Case A was chosen as the base case for all the sensitivity studies discussed in this section. Table 4 summarizes the results for the various sensitivity studies performed relative to Case A (base case) and includes a list of the parameters that were varied. In this table, the numerically predicted values for Sensor 1 and Sensor 7 at 3600 s after the release of helium are shown for each study and compared with those for Case A. It should be noted that in some cases, the effect of changing a certain parameter may be more pronounced during the dispersion phase or during the early release phase and that this effect may not be captured adequately in the table, which shows comparison at a single time value (3600 s). Each of the parametric study is discussed in more detail in the subsequent paragraphs.

Figure 12 shows the effect of changing the helium mass flux through the burner on the predicted helium volume fraction for sensors 1 and 7. The numerical predictions with the specified flow rate as in the experiments is shown with solid lines while the numerical predictions with 10 % higher mass flow rate is shown with dashed lines. For comparison, the experimental data is indicated with symbols. Orange color is used for sensor 1, while green color is used for sensor 7. Detailed comparison between numerical predictions and experimental data for all the sensors was discussed in the previous section. Since the burner cross-sectional area did not change between the two numerical simulations, increasing the mass flux rate resulted in helium flowing out at a higher velocity through the burner. Results indicate that increasing the mass flux through the burner increases the predicted volume fraction by as much as 7.4 %, for both sensors 1 and 7. Since the results are sensitive to the mass flux, accurate measurement of the mass flux through the burner for the duration of the experiment is necessary to obtain more accurate comparison between the data and numerical predictions.

The effect of changing the burner diameter on the predicted helium volume fraction is shown in Figure 13. Limited grid resolution in the region surrounding the burner may sometime result in a burner cross-section that is smaller or larger than that used in the experiments. When the cross-sectional area of the burner was reduced by 25 %, the predicted helium volume fraction increased by 2.5 % for both sensors 1 and 7. Note that the mass flux through the burner did not change in the two cases. Reducing the burner cross-sectional area resulted in an increase in the flow velocity so as to obtain a constant mass flux through the burner. This parametric study implicitly accounts for the reduction in burner diameter due to the effect of boundary layers. Note that the numerical simulations assumed a flat velocity profiles at the burner exit, and did not explicitly account for the effect of a boundary layer. The minor differences in the numerical predictions and experimental data can also be explained because of limitations in modeling the round cross-section of the burner with a square cross-section. The flow dynamics and air entrainment for a round buoyant jet can be significantly different from that of a square jet.

FDS uses the LES technique [15], [16] to model the dissipative processes that occur on length scales smaller than those that are resolved on the numerical grid. Following the analysis by Smagorinsky, the turbulent viscosity μ modeled as

$$\mu = \rho(C_s \Delta)^2 \left(2\bar{S}_{ij} \cdot \bar{S}_{ij} - \frac{2}{3}(\nabla \cdot \bar{u}) \right)^{\frac{1}{2}}, \quad (1)$$

where, ρ is the density, C_s is an empirical Smagorinsky constant, \bar{S}_{ij} is the symmetric rate-of-strain tensor, written using conventional tensor notation, Δ is the grid cell size and \bar{u} bulk fluid velocity vector. The material diffusivity D , was related to the turbulent viscosity through the turbulent Schmidt number Sc , assumed to be a constant for a given scenario, as shown below

$$(\rho D)_{LES} = \frac{\mu}{Sc}. \quad (2)$$

This material diffusion coefficient was used to model the diffusion of helium in the reduced scale garage experiment. In the buoyant helium plume and its immediate vicinity, the turbulent diffusion coefficient was larger than the binary diffusion coefficient computed from the Lennard Jones parameters and collision integrals. However in a large fraction of the computational domain, the flow was laminar, as the helium at the top of the compartment diffused towards the floor. In this region the computed turbulent diffusion coefficient could be smaller than the binary diffusion coefficient.

The effect of changing the turbulent Schmidt number (Equation 2) from 0.3 to 0.5 is shown in Figure 14. As the Schmidt number increases from 0.3 to 0.5, the helium volume fraction predicted at the location of sensor 7 increased by 2.3 % while that at the location of sensor 1 showed a small decrease, especially during the release phase. The effect of changing the Smagorinsky constant (Equation 1) from 0.2 to 0.12 (shown in Figure 15) on the predicted results indicate that the peak helium volume fraction can be higher by 10-12 % for both sensors 1 and 7 over the release and dispersion phase. Effect of including the baroclinic torque terms in the numerical simulation on the predicted volume fraction is illustrated in Figure 16, and the result indicate a change of less than 3%.

The location of the plumes will depend on the construction of the chasis and the release points under the vehicle. The effect of release location was partially captured by moving the burner from the center of the compartment (Case A) to the rear of the compartment (Case B). Comparison of the results for Case A and Case B are shown in Figure 17. Moving the burner towards the rear wall can change the entrainment of the air into the helium jet. However it appears that in this case the burner was sufficiently far from the rear wall (2.5 cm from the rear wall) so as to make a negligible change to the entrainment field. Results indicate that the helium volume fraction for sensors 1 and 7 were almost identical for the two cases. Since the jet velocity through the burner was relatively small (25 cm/s), this result was expected as the flow through the burner consists of a laminar low velocity helium plume ($Re < 100$, based on burner diameter) with air entrainment. Figure 18 shows the effect on helium volume fraction when the burner was moved close to the ceiling (Case D with a one hour release), instead of resting on the floor (Case A). Moving the burner close to the ceiling had a much more significant effect on the measured concentrations, since it reduced the distance and time available for entrainment of air into the helium plume. As a result, the helium concentration measured for sensor 1 was significantly lower and for sensor 7 significantly higher, when the burner was moved close to the ceiling.

The effect of limiting the size and shape of the computational domain on predicted helium volume fraction has been shown in and Figure 19. Results from a smaller computational domain where “free” flow boundary conditions were

applied on the flow through the hole was compared with those from a larger computational domain where boundary conditions were imposed away from the hole. Since the computational domain shown was smaller, the computational cost was proportionately smaller. The disadvantage of using a smaller domain is the inability to capture all the physics of the flow-field through the hole with an “open” boundary condition. Note that the flow field through the hole can be quite complex as it exhibits an oscillating flow (gurgling) and can sometimes affect the measured helium concentration. Results shown in Figure 19 indicate that the effect of the modified boundary condition was to reduce the helium volume fraction for sensors 1 and 7 by less than 2 %.

The effect of changing the size of the hole in the front wall on the predicted helium volume fraction is shown in Figure 20. This figure compares simulation results for a hole size of 2.34 cm x 2.32 cm (cross-sectional area 5.43 cm²) with those for a hole size of 1.56 cm x 2.32 cm (cross-sectional area 3.62 cm²). Note that in the experiments the hole was 2.4 cm x 2.4 cm with a cross-sectional area of 5.76 cm². The difference in the size of the hole between the experiment and numerical simulations was due to limitations and restrictions on the grid density used in the simulations. It should also be noted that the vertical location of the hole or its size in the vertical direction (2.32 cm) did not change for the two simulations. Results indicate that the predicted volume fraction was not very sensitive to the size of the hole and that only minor differences were observed during the dispersion phase (less than 2.5 %). This result indicates that the size of the leak was not a very important parameter. For a typical two-car residential garage, the size of the leaks are not known a-priori, and this result has important ramifications when constructing models for simulating dispersion and mixing in garages with unknown leaks.

The size of the leak does not have a large effect on the predicted gas concentration, but the location of the leaks has a large effect on mixing and dispersion. Figure 21 compares the predicted helium volume fractions for Case A (single leak in the center of the compartment) with Case C (two holes in the front wall, one at the top and one at the bottom). Note that the area of the leaks in the two cases that have been compared is quite different, but it has also been pointed out (discussion for Figure 20) that the size of the leaks does not have a significant effect on the computed results. The results shown in Figure 21 indicate that the location of the leaks has a very large effect on the gas concentration inside a compartment, while the size of the leak has a smaller effect on the predicted values.

A typical simulation of hydrogen dispersion in a compartment would require a fine mesh around the burner to capture the buoyant jet flow and air entrainment. Fine mesh is also needed in the vertical direction to adequately capture the diffusion of the gases from the ceiling towards the floor, as well as in the area around the leaks to fully resolve the dynamics of the fluid flow in this region. The computational cost for performing simulations of hydrogen release and dispersion

is a function of the grid density used in the simulations. For a single processor calculation, increasing the grid density can result in prohibitively large computational costs and memory requirements for the CPU. A 48 x 64 x 64 cartesian mesh was used for all the simulations that have been described so far. The grid was concentrated in the region around the burner with a minimum grid spacing of 7.8 mm, while the grid was uniform in the vertical direction with grid spacing of 1.16 cm. Increasing the mesh density in the plume region and through the leaks can improve the comparison between numerical simulations and experimental data. The grid that was chosen for the current study was a compromise between the desired accuracy and the computational cost of the simulation. Since the sensors were located outside the plume region, the grid used in the simulations was adequate for predicting the measured helium volume fraction. A more finely resolved mesh would be needed, if the sensors were located inside the plume. Figure 22 shows the effect of changing the mesh density in the vertical direction from 64 evenly spaced grid points (grid size of 1.16 cm) to 48 evenly spaced points (grid size of 1.55 cm). Results indicate that coarse mesh and fine mesh solutions were relatively close during the release phase, however, the relative difference between the coarse mesh and fine mesh solution during the dispersion phase was approximately 7.5 %. This indicates that the helium volume fraction will increase as the grid density increases and will better approximate the experimental data. The effect of coarsening the mesh in the horizontal direction (y direction) from 64 grid points to 48 grid points is shown in Figure 23. It should be noted that coarsening the mesh in the horizontal direction can change the entrainment pattern, but also has the un-wanted effect of changing the size of the burner and that this can affect the results of this resolution study.

The effect of changing the buoyant gas from helium to hydrogen on the predicted volume fraction is shown in Figure 24. In each case the volume flow rate of the buoyant gas leaving the nozzle was kept constant. Results indicate that there was a negligible change in the predicted volume fractions. This result is consistent with the data presented by Swain et al. [4] Simulation results, comparison with experimental data and the sensitivity study indicates that the FDS software can be reliably used for simulating the release, mixing and dispersion of both hydrogen and helium in partially enclosed spaces.

5. Summary and Conclusions

Numerical simulations using the Fire Dynamics Simulations (FDS) have been performed to predict the mixing and dispersion of helium and hydrogen in partially enclosed compartments. Experiments were conducted in a reduced scale enclosure with idealized leaks to provide a database for model validation. Simulations of the experimental setup accurately predicted the observed trend for various burner locations, leak configuration and duration of release. The difference between the experimentally measured peak concentrations and numerical simulation results, averaged over all the sensors and the various cases studied in this paper was found to be 2.3%. Sensitivity of the computed results on

various model parameters was determined. It was noted that the size of the leak (hole in the garage) had a small effect, but the location of the leaks had a very large effect on the predicted concentration. Other parameters that were found to have a significant effect on the predicted concentration included mass flux rate through the burner, location of the burner and the value of the Smagorinsky constant used in the simulations. The simulations did not account for thermal effects, role of an external wind, or clutter in the garage, which can have a significant effect on the predicted concentrations.

6. Acknowledgement

The authors would like to thank Marco Fernandez for his help in building the reduced scale garage and conducting the experiments.

7. References

1. Hydrogen Technology, Aline Leon, Editor, Springer 2008.
2. Wolfgang Breitung, Safety Analysis of Hydrogen Vehicles and Infrastructure, in Hydrogen Technology, Aline Leon, Editor, Springer, 2008.
3. Michael R. Swain, Eric S. Grilliot and Matthew N. Swain, Advances in hydrogen energy, New York, Kluwer Academic Publishers, Plenum Press, Dordrecht, p. 163-173, 2000.
4. Michael R. Swain, Patrick Filoso, Eric S. Grilliot and Matthew N. Swain, International Journal of Hydrogen Energy, 28, 229-248, 2003.
5. Dagba, Y., Perette, L., Venetsanos, A. G., Description of INERIS-Test6 experiment and requirements for corresponding blind SBEP in the framework of the InsHyde internal project, HYSAFE report, 2005.
6. A. G. Venetsanos, E. Papanikolaou, M. Delichatsios, J. Garcia, O. R. Hansen, M. Heitsh, A. Huser, W. Jahn, T. Jordan, J-M. Lacomme, H.S. Ledin, D. Makarov, P. Middha, E. Studer, A.V. Tchouvelev, A. Teodorczyk, F. Verbecke, M.M. van der Voort, An Inter-comparison exercise on the capabilities of CFD models to predict the short and long term distribution and mixing of Hydrogen in a Garage, 2nd International Conference on Hydrogen Safety, 2007.
7. J. Zhang, J. Hereid, M. Hagen, D. Bakirtzis, M. A. Delichatsios and A. G. Venetsanos, Numerical Studies of Dispersion and Flammable Volume of Hydrogen in Enclosures, 2nd International Conference on Hydrogen Safety, 2007.
8. A. V. Tchouvelev, J. DeVaal, Z. Cheng, R. Corfu, R. Rozek and C. Lee, CFD Modeling of Hydrogen Dispersion Experiments for SAE J2578 Test Methods Development, 2nd International Conference on Hydrogen Safety, 2007.
9. J. M. Lacomme, Y. Dagba, D. Jamois, L. Perrette, C.H. Proust, Large-scale Hydrogen Release in an Isothermal Confined Area, 2nd International Conference on Hydrogen Safety, 2007.
10. Michael R. Swain and Jeremy Shriber : Energy & Fuels, 12,83-89, 1998.

11. Robert Schefer and Bill Houf, "Experimental Measurement to Characterize the Thermal and Radiation Properties of an Open-flame Hydrogen Plume," 15th Annual Hydrogen Conference and Hydrogen Expo, 2006.
12. Alejandro Molina, Robert W. Schefer and William G. Houf, Radiative fraction and optical thickness in large-scale hydrogen jet fires, Proceedings of the Combustion Institute, 31, 2565-2572, 2007.
13. W. Breitung, G. Necker, B. Kaup, A. Vesper, Numerical Simulation of Hydrogen Release in a Private Garage, Proceedings of HypothesisIV, 2001.
14. Dennis Barley, Keith Gawlik, Jim Ohi and Russell Hewett, Buoyancy Driven Ventilation of Hydrogen from a Residential Garage, CTFCA-DOE H₂ Safety Meeting, 2007.
15. "Fire Dynamics Simulator (Version 5) User's Guide," Kevin McGrattan, Bryan Klein, Simo Hostikka, Jason Floyd, NIST Special Publication 1019-5, 2008.
16. "Fire Dynamics Simulator (Version 5) Technical Reference Guide," Kevin McGrattan, Simo Hostikka, Jason Floyd, Howard Baum, Ronald Rehm, Randall McDermott, NIST Special Publication 1018-5, 2008.
17. William Pitts, Kuldeep Prasad Jiann Yang, Experimental Characterization and Modeling of Helium Dispersion in a 1/4 –Scale Two-Car Residential Garage, submitted, 3rd International Conference on Hydrogen Safety, 2009.
18. Kuldeep Prasad, Nelson Bryner, Matthew Bundy, Thomas Cleary, Anthony Hamins, Nathan Marsh, William Pitts, Jiann Yang, Numerical Simulation of Hydrogen Leakage and Mixing in Large Confined Spaces, Proceedings of the NHA Annual Hydrogen Conference, 2008
19. Steven J. Emmerich, Joshua E. Gorfain, Mike Huang, Cynthia Howard-Reed, Air and Pollutant Transport from Attached Garages to Residential Living Spaces, NISTIR 7072, 2003
20. "User's Guide for Smokeview Version 5-A Tool for Visualizing Fire Dynamics Simulation Data, Glenn P. Forney, NIST Special Publication 1017-1, 2008.

List of Tables

Table 1. Sensor number and location (height above floor used to measure the helium volume fraction in the compartment.	17
Table 2. Summary of burner configuration, release point (m), leak configuration, leak location (m) and duration of release (s) for the helium release study. ..	17
Table 3. Percentage accuracy of the numerical predictions relative to the experimental data at the point when the helium flow through the burner was stopped (3600 s for Case A, B and C and 14400 s for Case D).....	18
Table 4. Percentage change in helium volume fraction computed at the location of Sensor 1 and Sensor 7 for the various sensitivity studies performed relative to Case A (Base Case).....	18

List of Figures

Figure 1. Photograph of the experimental setup used for the helium dispersion experiments, showing the burner, sensor location and size/shape of the hole in the front wall of the compartment.....	19
Figure 2. Schematic diagram of the experimental set-up used for mixing and dispersion simulations of highly buoyant gases.....	20
Figure 3. Helium volume fraction at 1800 s after the release of helium through a burner located in the center of the compartment close to the floor, while the leak consisted of a single hole located in the front wall of the compartment.	21
Figure 4. Density contours at 1800 s after the release of helium through a burner located in the center of the compartment close to the floor, while the leak consisted of a single hole located in the front wall of the compartment.....	22
Figure 5. Velocity vectors color coded with helium volume fraction at 1800 s after the release of helium through a burner located in the center of the compartment close to the floor. The velocity field close to the burner and the plume region is shown indicating the entrainment of air into the helium plume.....	23
Figure 6. Integrated values (over the cross-sectional area) of mass flow rate through the burner (black curve) and the hole (red curve), plotted as a function of time.....	24
Figure 7. Flow induced pressure perturbation plotted as a function of time at three heights in the compartment.....	24
Figure 8. Comparison of experimentally measured helium concentrations (symbols) with predicted values (lines) at seven sensor locations placed at various heights. Helium was released for one hour through a burner located in the center of the compartment, close to the floor, while the leak consisted of a single hole located in the front wall of the compartment (Case A).	25
Figure 9. Comparison of experimentally measured helium concentrations (symbols) with predicted values (lines) at seven sensor locations placed at various heights. Helium was released through a burner located in the rear of	

the compartment, close to the floor, while the leak consisted of a single hole located in the center of the compartment (Case B).....	26
Figure 10. Comparison of experimentally measured helium concentrations (symbols) with predicted values (lines) at seven sensor locations placed at various heights. Helium was released through a burner located in the center of the compartment, close to the floor, while the leak consisted of two holes, located at the top and bottom on one of the side walls of the compartment (Case C).	27
Figure 11. Comparison of experimentally measured helium concentrations (symbols) with predicted values (lines) at seven sensor locations placed at various heights. Helium was released through a burner located in the center of the compartment, close to the ceiling, while the leak consisted of a single hole located in the center of the compartment (Case D).....	28
Figure 12. Effect of increasing the helium mass flux rate through the burner on the predicted helium volume fraction plotted as a function of time.	29
Figure 13. Effect of changing the burner diameter on the predicted helium volume fraction plotted as a function of time. Mass flux rate was not changed when the nozzle diameter was changed.....	29
Figure 14. Effect of changing Schmidt number from 0.3 to 0.5 on the computed helium volume fraction.	30
Figure 15. Effect of changing Smagorinsky constant from 0.2 to 0.12 on predicted helium volume fraction.	30
Figure 16. Effect of including the baroclinic torque terms on the computed helium volume fraction.	31
Figure 17. Effect of moving the location of the burner from the center of the compartment to the rear of the compartment on computed helium volume fraction.	31
Figure 18. Effect of changing the release location from close to the floor to close to the ceiling on predicted helium concentration.	32
Figure 19. Effect of changing the size of the computational domain on helium volume fraction.	32
Figure 20. Effect of changing the size of the hole (leak) on the computed helium volume fraction.	33
Figure 21. Effect of changing the location of the holes on predicted helium volume fraction at two heights in the compartment.....	33
Figure 22. Effect of changing the mesh density in the vertical direction on the predicted helium volume fraction.	34
Figure 23. Effect of changing grid density in the horizontal direction on the predicted helium volume fraction.	34
Figure 24. Effect of changing the gas released from helium to hydrogen on the predicted volume fraction. The volume flow rates were kept constant for the two cases.	35

Table 1. Sensor number and location (height above floor used to measure the helium volume fraction in the compartment.

Sensor #	Height above floor (m)
1	0.093
2	0.185
3	0.276
4	0.372
5	0.446
6	0.559
7	0.650

Table 2. Summary of burner configuration, release point (m), leak configuration, leak location (m) and duration of release (s) for the helium release study.

Scenario	Burner Location	Release location (m)	Leak on front wall	Leak location (m)	Release time (s)
Case A	Center of box, resting on floor	(0.0,0.75,0.21)	One hole in center	(0.0,0.0,0.375)	3600
Case B	Rear of box, resting on floor	(0.0,1.48,0.21)	One hole in center	(0.0,0.0,0.375)	3600
Case C	Center of box, resting on floor	(0.0,0.75,0.21)	Two hole, top,bottom	(0.0,0.0,0.025) (0.0,0.0,0.725)	3600
Case D	Center of box close to ceiling	(0.0,0.75,0.72)	One hole in center	(0.0,0.0,0.375)	14400

Table 3. Percentage accuracy of the numerical predictions relative to the experimental data at the point when the helium flow through the burner was stopped (3600 s for Case A, B and C and 14400 s for Case D).

	Percentage accuracy relative to experimental data							
	Sensor 1	Sensor 2	Sensor 3	Sensor 4	Sensor 5	Sensor 6	Sensor 7	Case Average
Case A	3.4	2.7	2.9	3.3	4.0	3.9	2.8	3.3
Case B	3.4	3.0	2.3	2.4	2.4	2.2	0.2	2.2
Case C	0.0	0.9	4.3	4.3	9.3	7.8	5.6	4.6
Case D	-1.6	-1.3	-1.4	-1.0	-1.0	-0.5	0.0	-0.9
Sensor Average	1.3	1.3	2.0	2.2	3.7	3.3	2.1	2.3

Table 4. Percentage change in helium volume fraction computed at the location of Sensor 1 and Sensor 7 for the various sensitivity studies performed relative to Case A (Base Case).

Scenario	Sensor 1	Sensor 7
1) Increase mass flux by 10 %	8.0 %	6.6 %
2) Reduce burner diameter by 25 % ³	2.7 %	2.2 %
3) Increase Schmidt number from 0.3 to 0.5	-2.0 %	2.2 %
4) Change Smagorinsky constant from 0.2 to 0.12	14.5 %	8.2 %
5) Include baroclinic torque terms	0.0 %	3.8 %
6) Move burner horizontally (Case A vs. B)	0.0 %	2.6 %
7) Move burner vertically (Case A vs. D)	-14.8 %	15.0 %
8) Boundary condition at the hole	1.8 %	1.3 %
9) Reduce leak area by 25 %	0.0 %	0.2 %
10) Change location of the leaks (Case A vs. C)	-49.5 %	-25.2 %
11) Reduce resolution (vertical direction)	-0.3 %	-1.3 %
12) Reduce resolution (horizontal direction)	4.5 %	2.6 %
13) Change gas from helium to hydrogen ⁵	1.2 %	-0.4 %

³ Maintain constant mass flux



**Front plate of
compartment** **Sensors** **Burner** **Hole**

Figure 1. Photograph of the experimental setup used for the helium dispersion experiments, showing the burner, sensor location and size/shape of the hole in the front wall of the compartment.

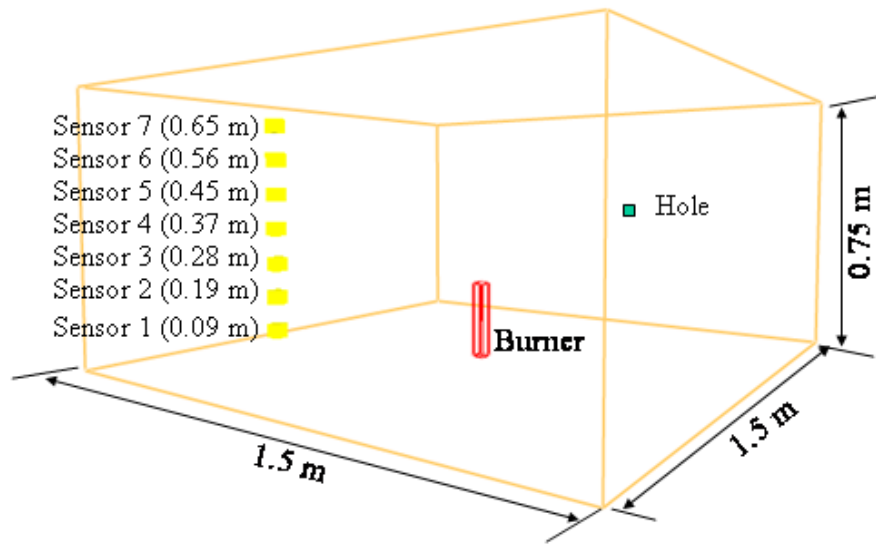


Figure 2. Schematic diagram of the experimental set-up used for mixing and dispersion simulations of highly buoyant gases.

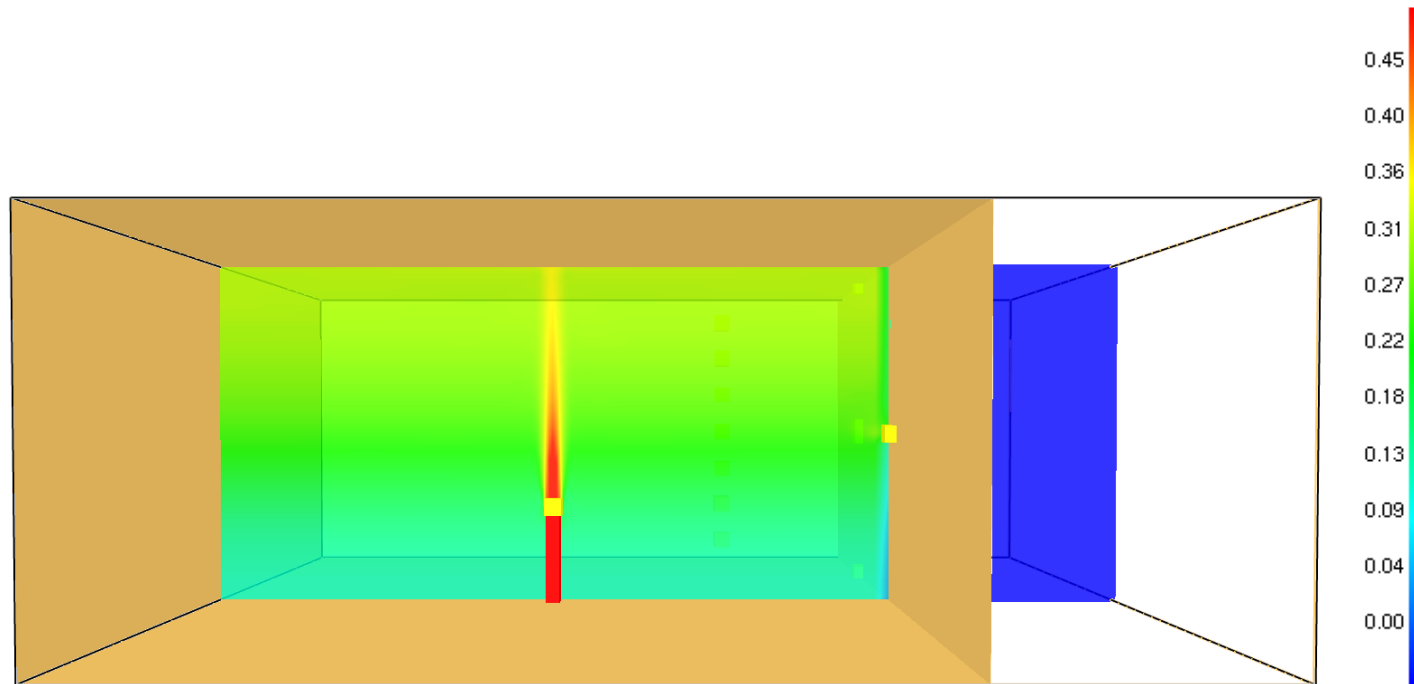


Figure 3. Helium volume fraction at 1800 s after the release of helium through a burner located in the center of the compartment close to the floor, while the leak consisted of a single hole located in the front wall of the compartment.

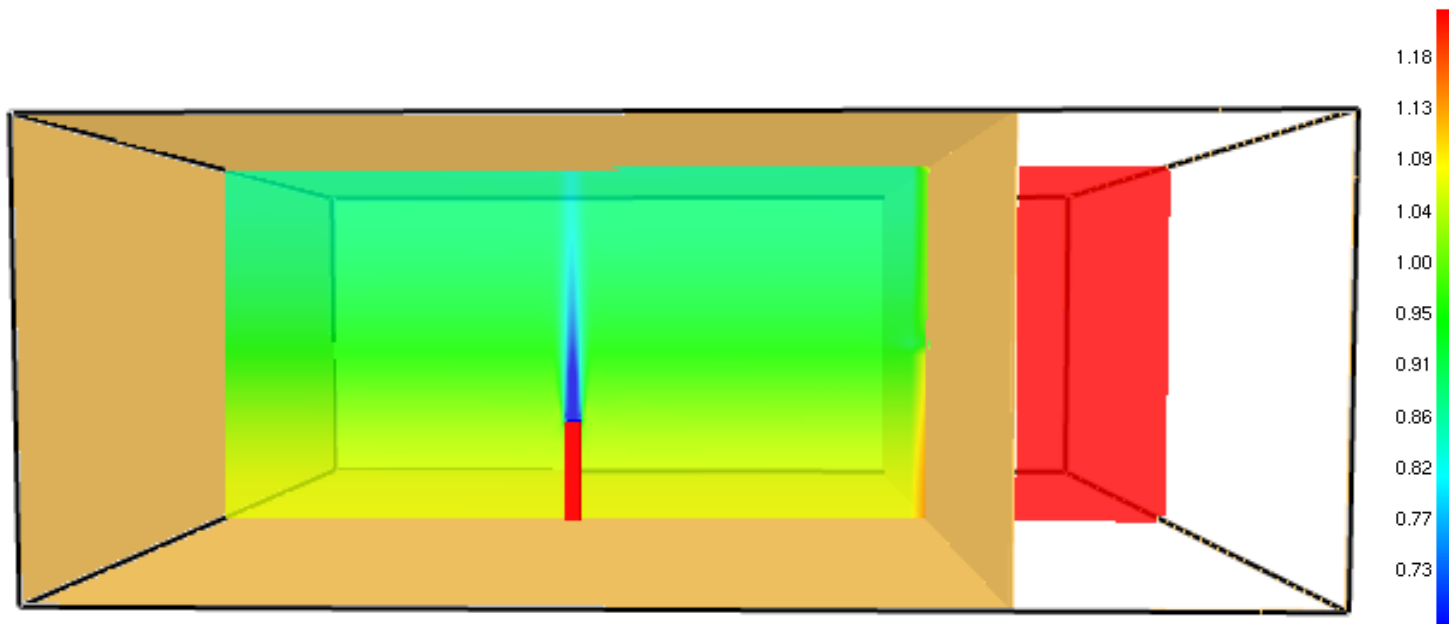


Figure 4. Density contours at 1800 s after the release of helium through a burner located in the center of the compartment close to the floor, while the leak consisted of a single hole located in the front wall of the compartment.

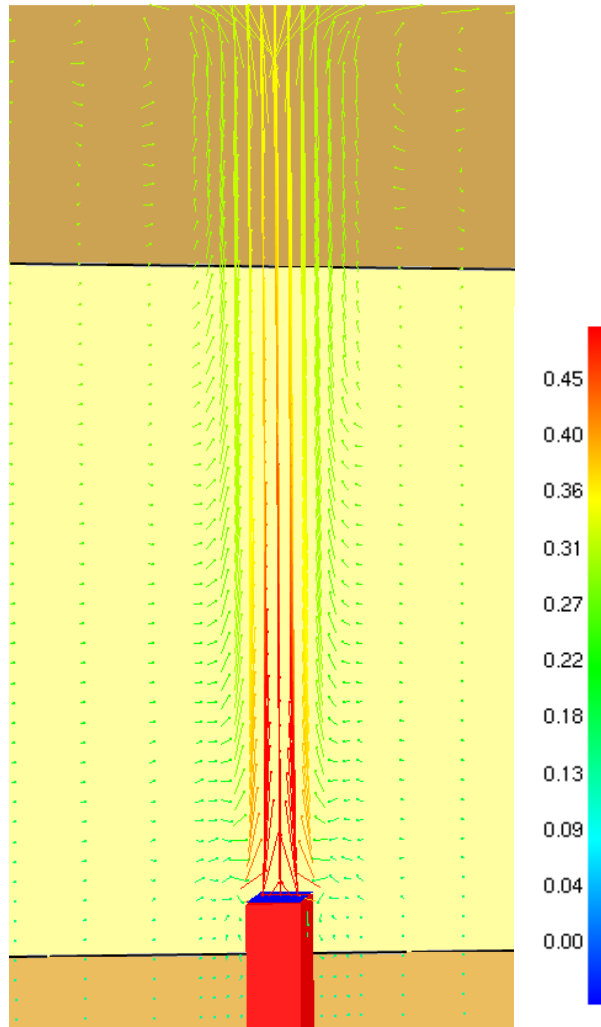


Figure 5. Velocity vectors color coded with helium volume fraction at 1800 s after the release of helium through a burner located in the center of the compartment close to the floor. The velocity field close to the burner and the plume region is shown indicating the entrainment of air into the helium plume.

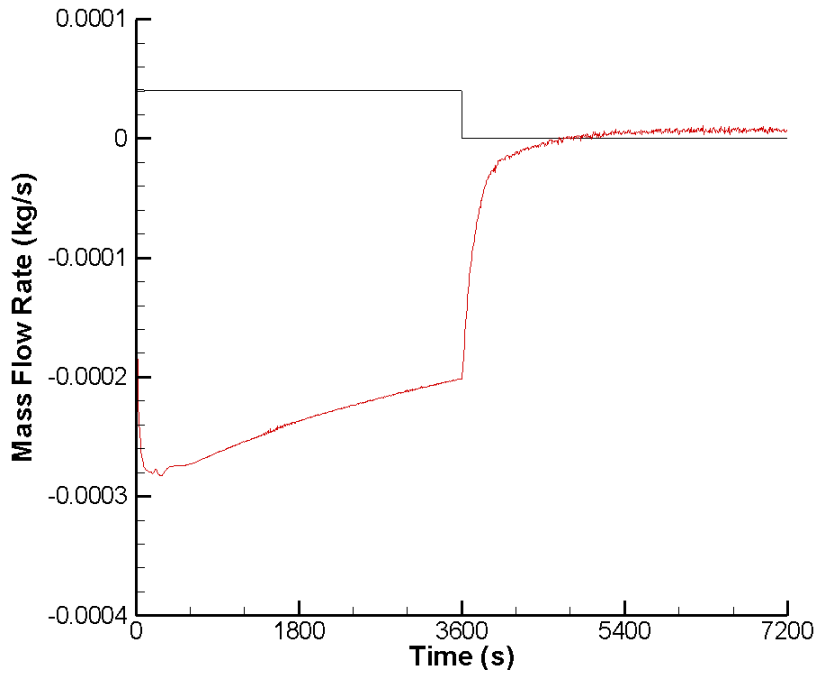


Figure 6. Integrated values (over the cross-sectional area) of mass flow rate through the burner (black curve) and the hole (red curve), plotted as a function of time.

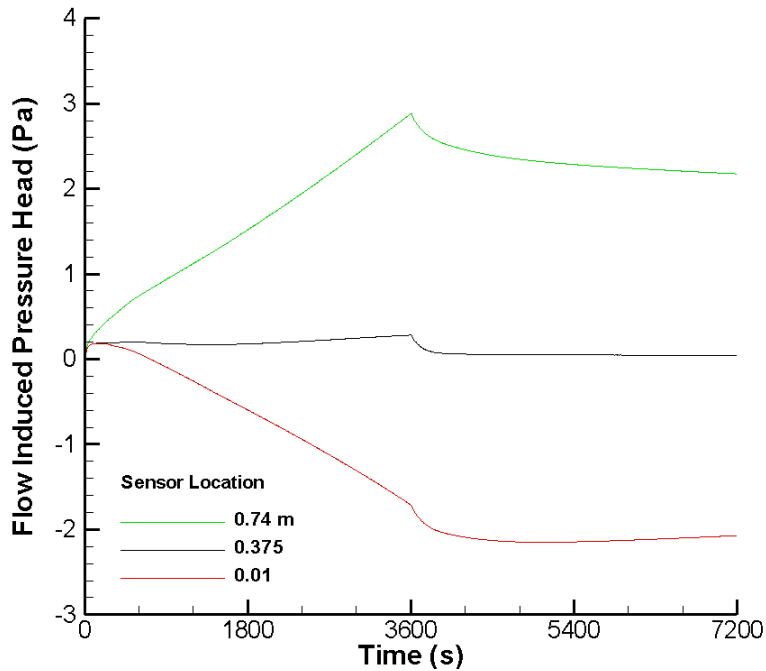


Figure 7. Flow induced pressure perturbation plotted as a function of time at three heights in the compartment.

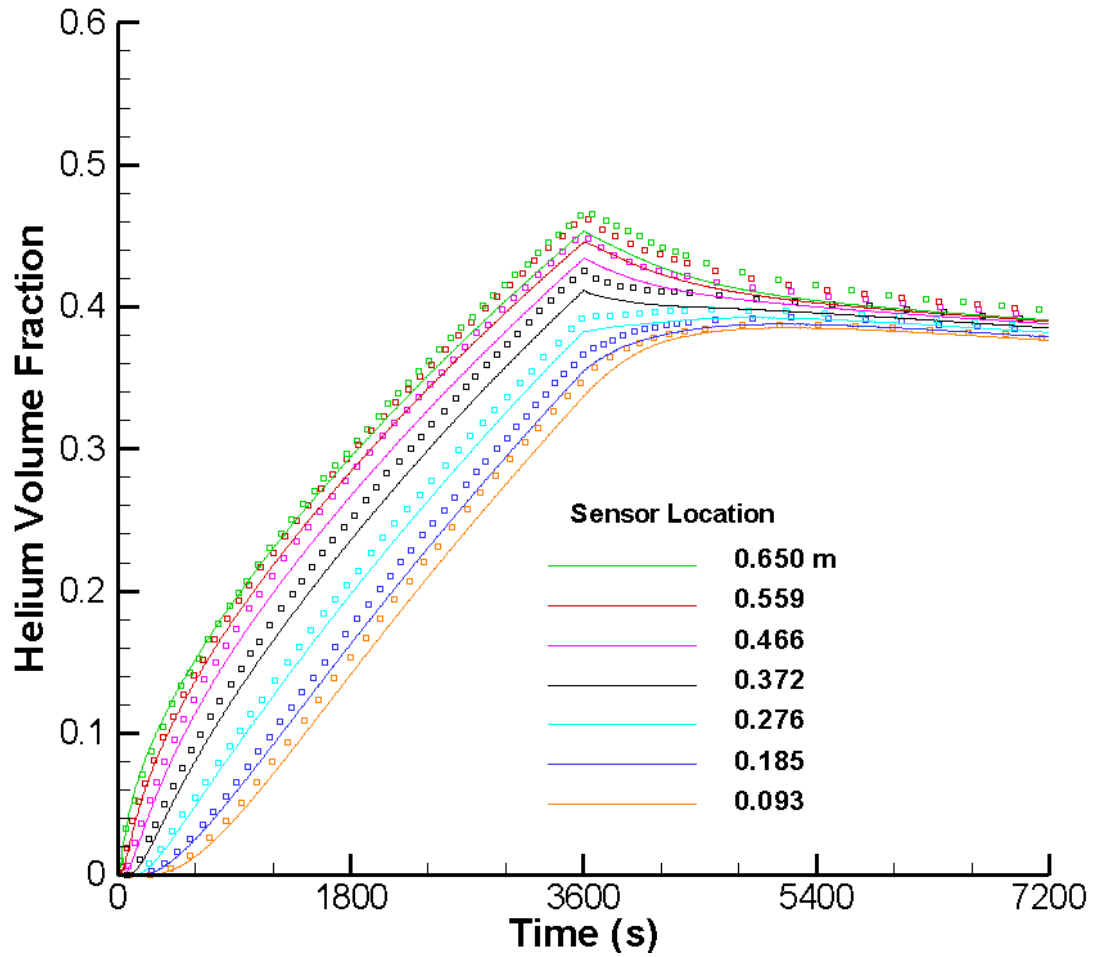


Figure 8. Comparison of experimentally measured helium concentrations (symbols) with predicted values (lines) at seven sensor locations placed at various heights. Helium was released for one hour through a burner located in the center of the compartment, close to the floor, while the leak consisted of a single hole located in the front wall of the compartment (Case A).

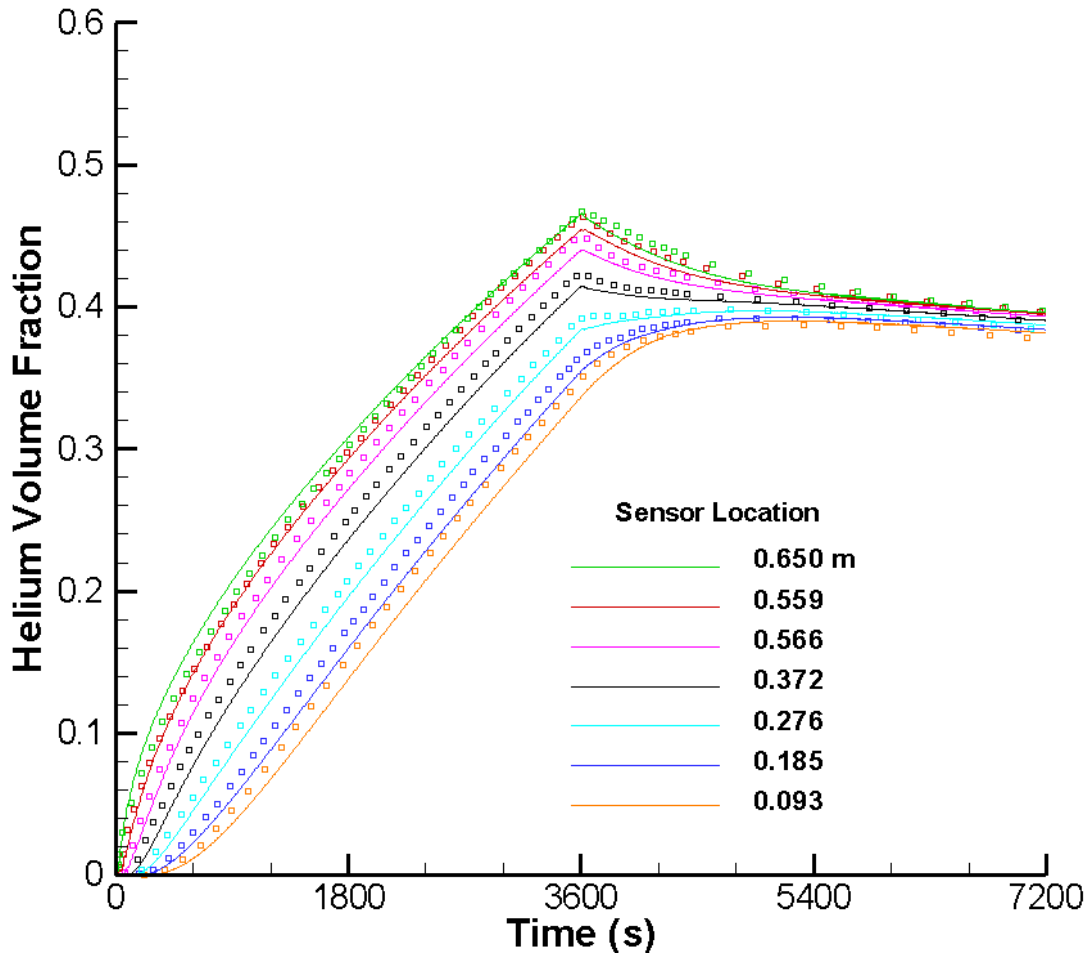


Figure 9. Comparison of experimentally measured helium concentrations (symbols) with predicted values (lines) at seven sensor locations placed at various heights. Helium was released through a burner located in the rear of the compartment, close to the floor, while the leak consisted of a single hole located in the center of the compartment (Case B).

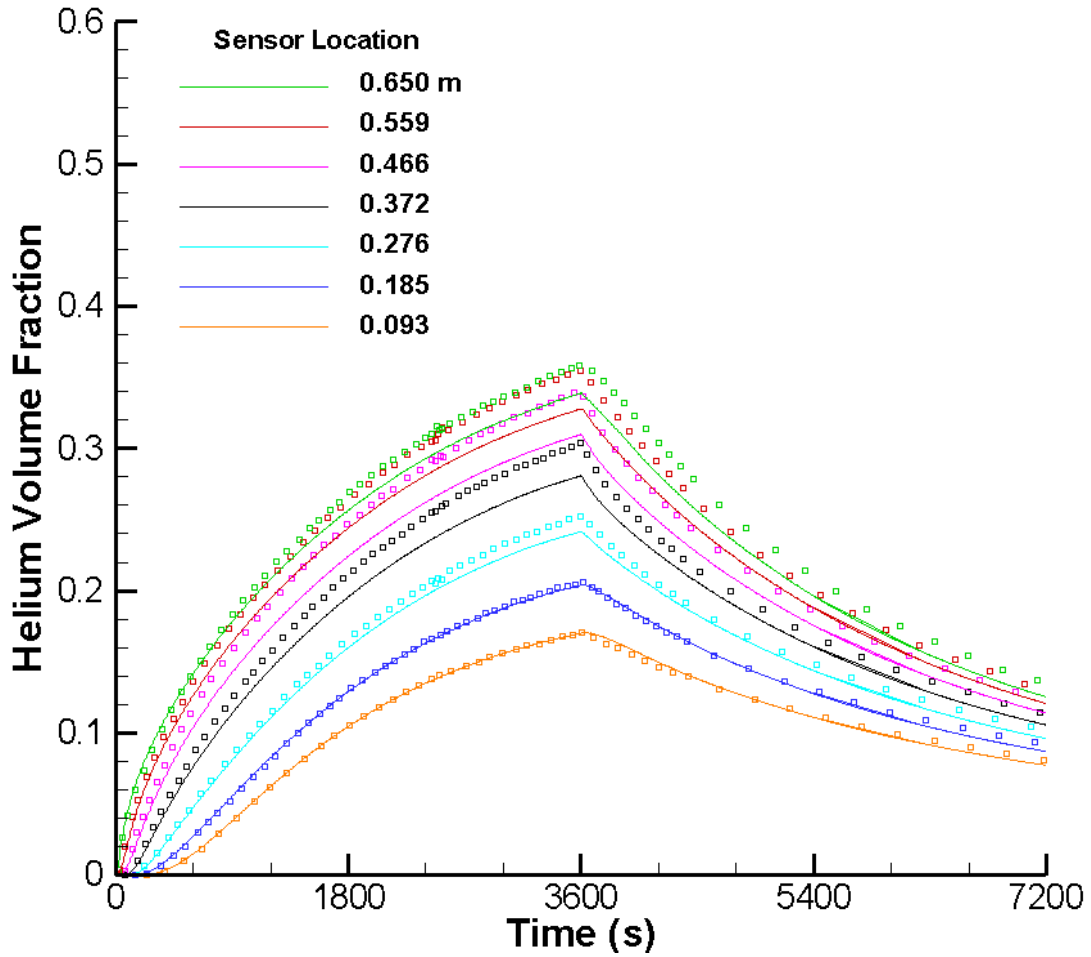


Figure 10. Comparison of experimentally measured helium concentrations (symbols) with predicted values (lines) at seven sensor locations placed at various heights. Helium was released through a burner located in the center of the compartment, close to the floor, while the leak consisted of two holes, located at the top and bottom on one of the side walls of the compartment (Case C).

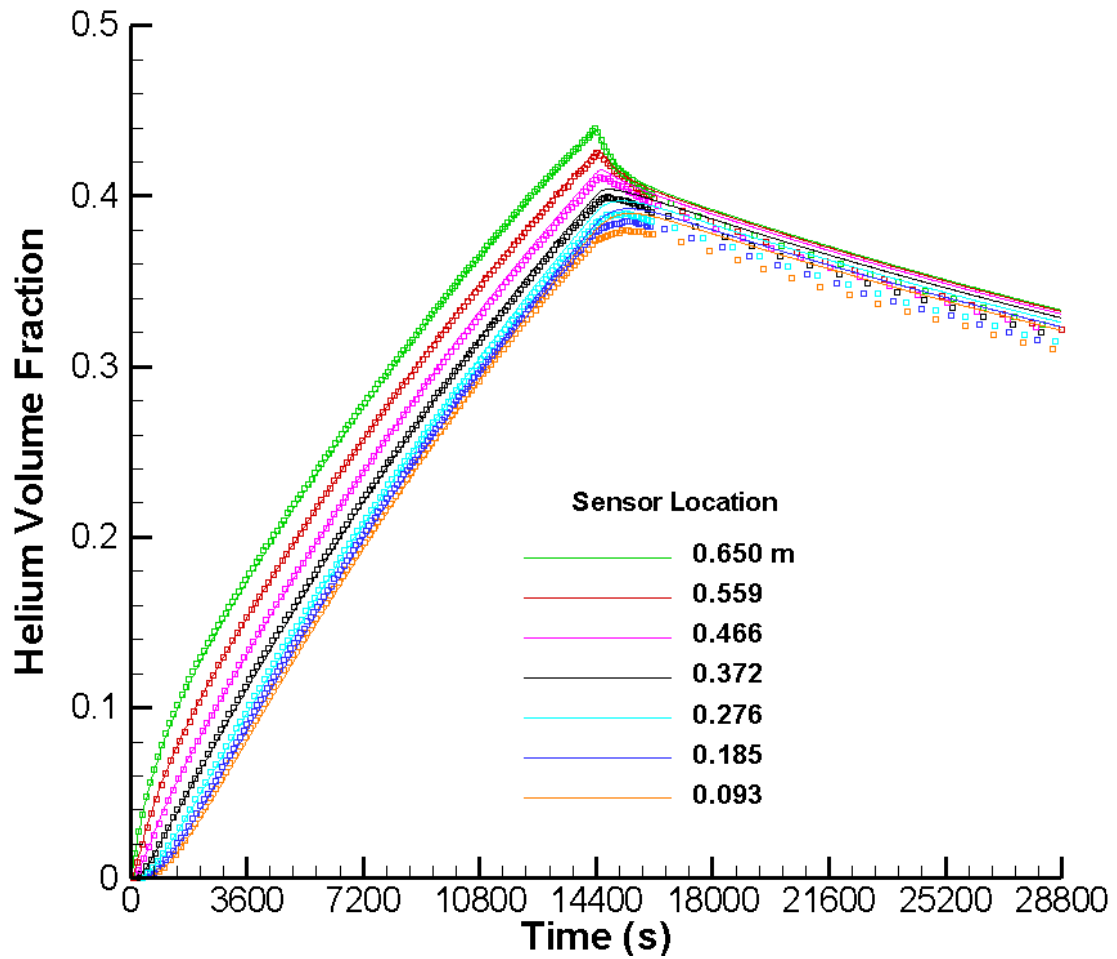


Figure 11. Comparison of experimentally measured helium concentrations (symbols) with predicted values (lines) at seven sensor locations placed at various heights. Helium was released through a burner located in the center of the compartment, close to the ceiling, while the leak consisted of a single hole located in the center of the compartment (Case D).

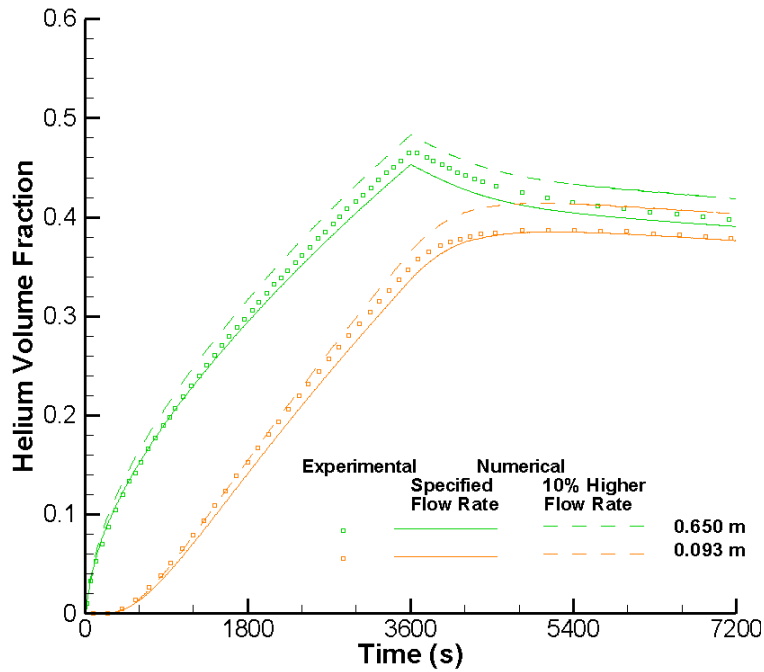


Figure 12. Effect of increasing the helium mass flux rate through the burner on the predicted helium volume fraction plotted as a function of time.

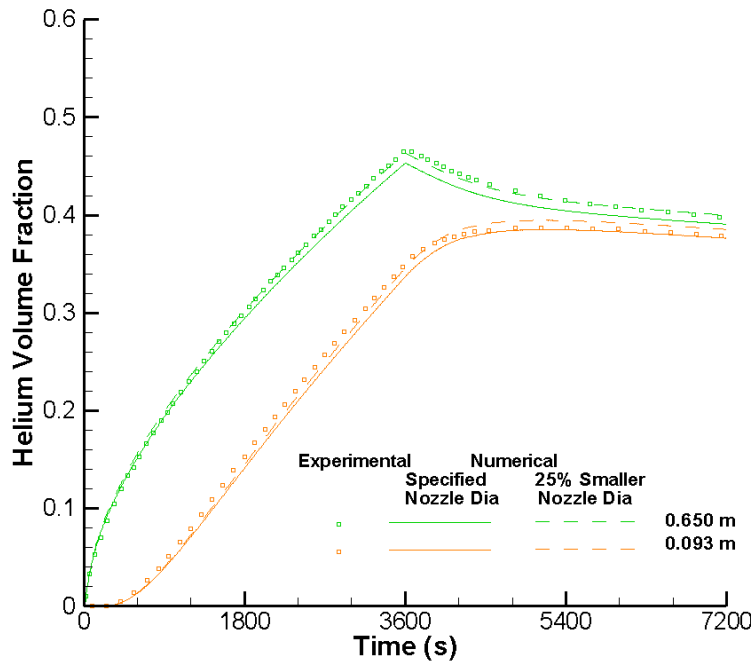


Figure 13. Effect of changing the burner diameter on the predicted helium volume fraction plotted as a function of time. Mass flux rate was not changed when the nozzle diameter was changed.

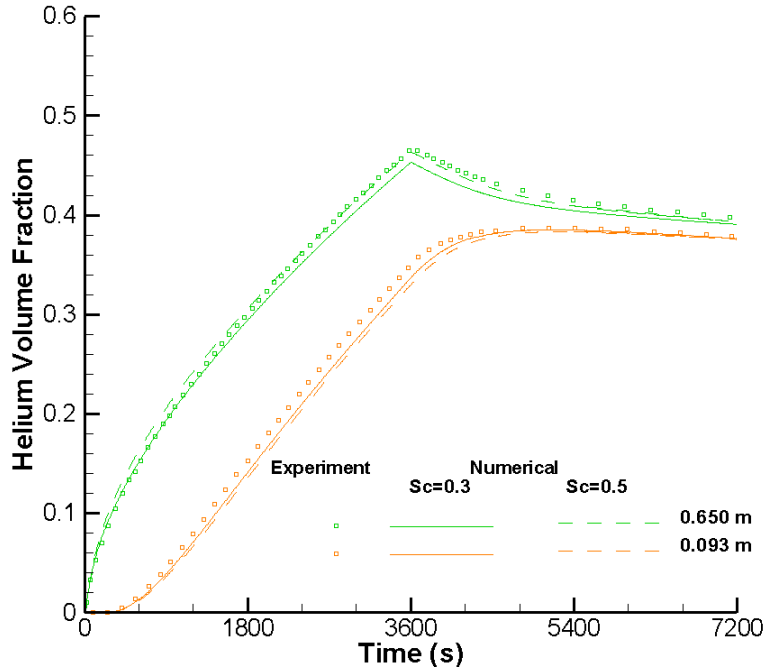


Figure 14. Effect of changing Schmidt number from 0.3 to 0.5 on the computed helium volume fraction.

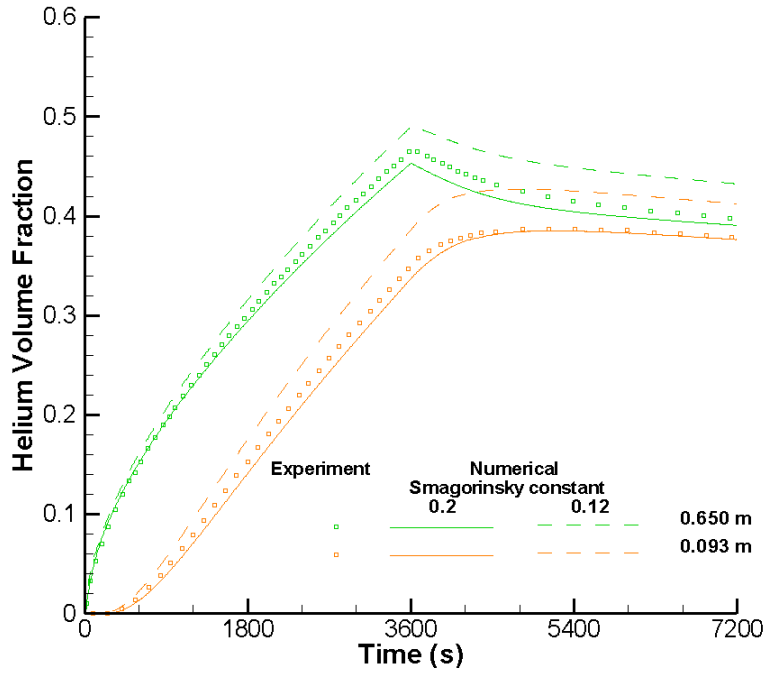


Figure 15. Effect of changing Smagorinsky constant from 0.2 to 0.12 on predicted helium volume fraction.

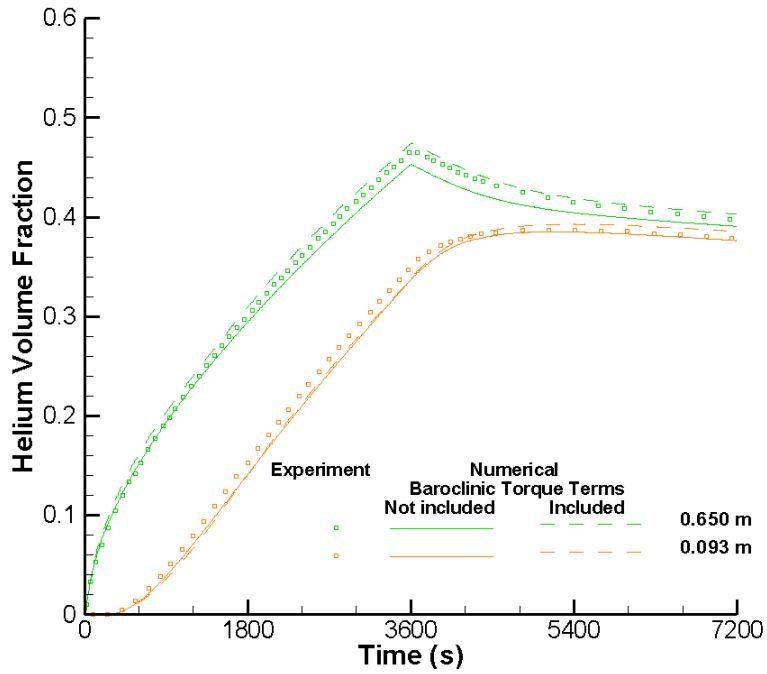


Figure 16. Effect of including the baroclinic torque terms on the computed helium volume fraction.

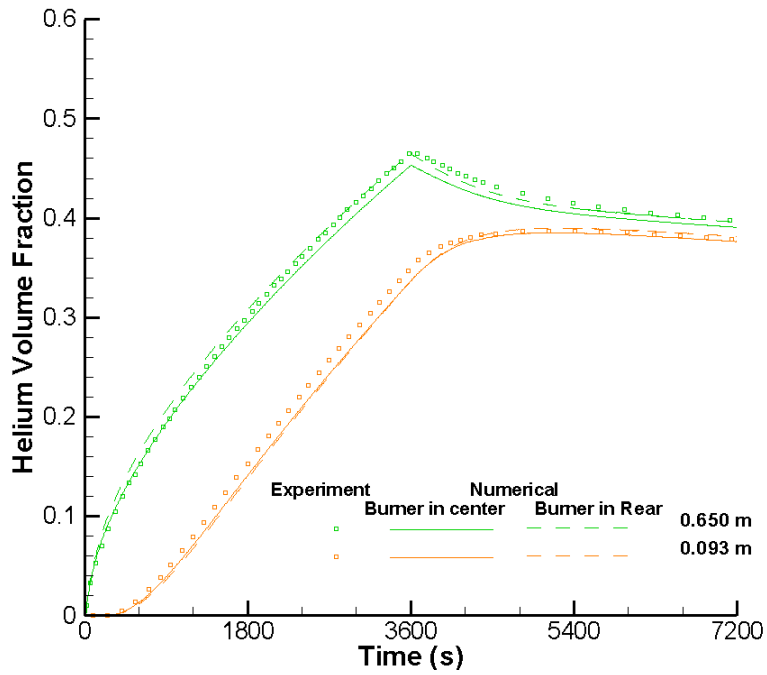


Figure 17. Effect of moving the location of the burner from the center of the compartment to the rear of the compartment on computed helium volume fraction.

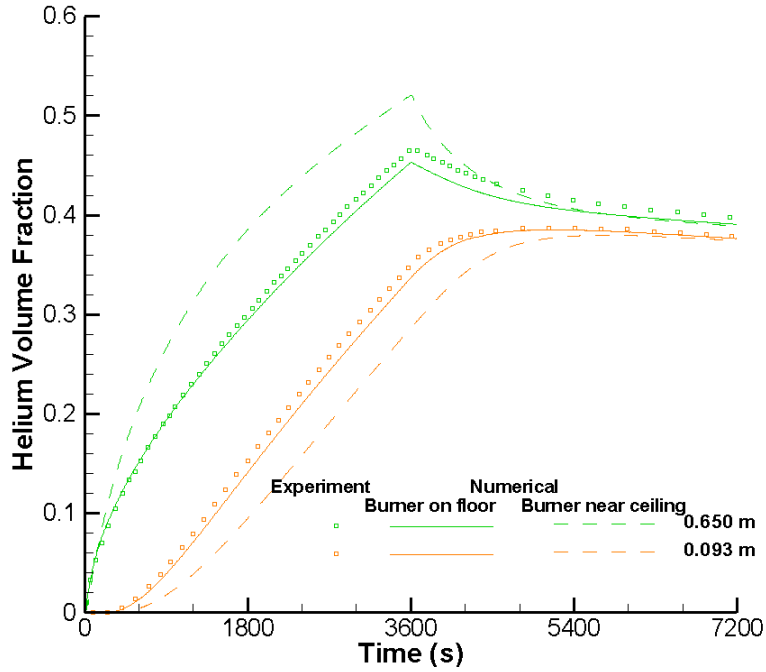


Figure 18. Effect of changing the release location from close to the floor to close to the ceiling on predicted helium concentration.

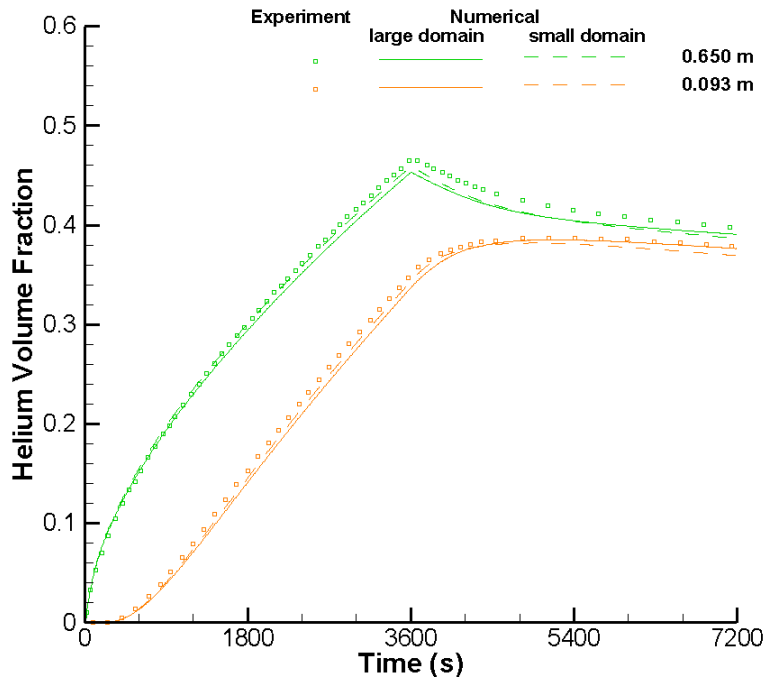


Figure 19. Effect of changing the size of the computational domain on helium volume fraction.

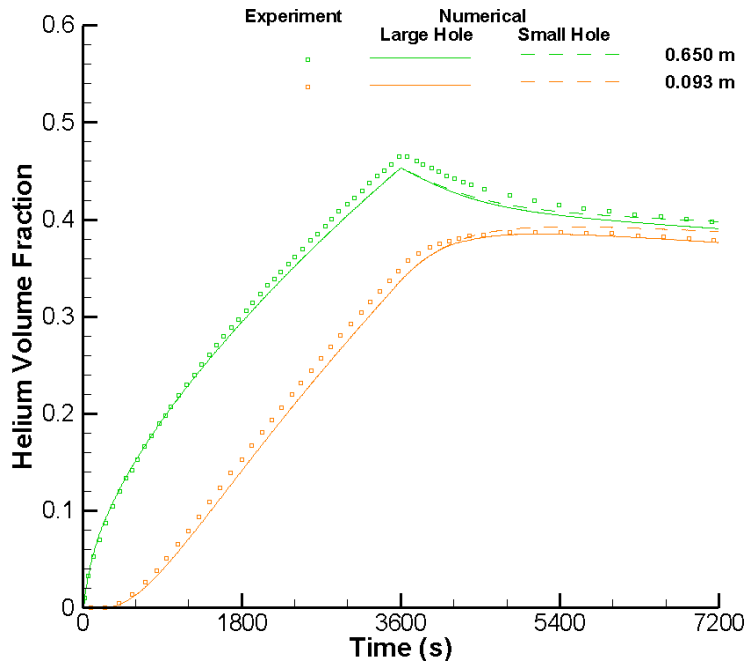


Figure 20. Effect of changing the size of the hole (leak) on the computed helium volume fraction.

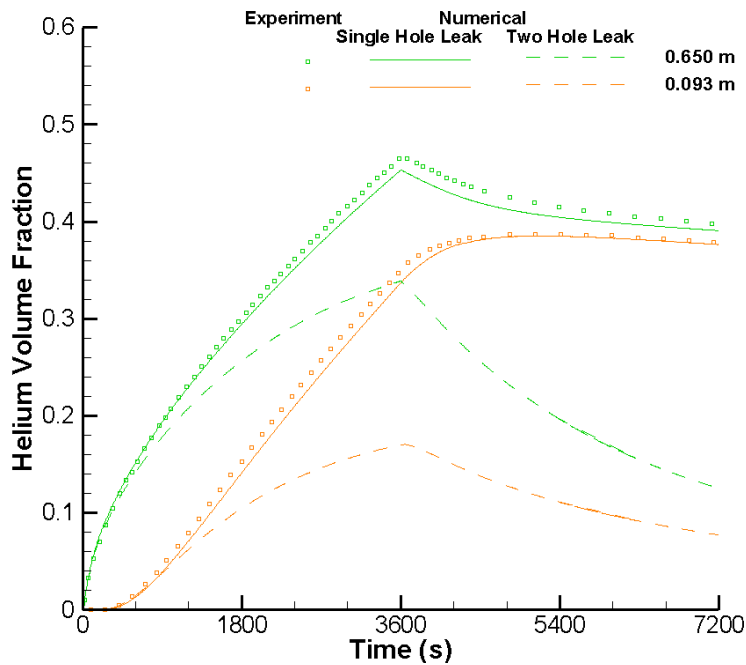


Figure 21. Effect of changing the location of the holes on predicted helium volume fraction at two heights in the compartment.

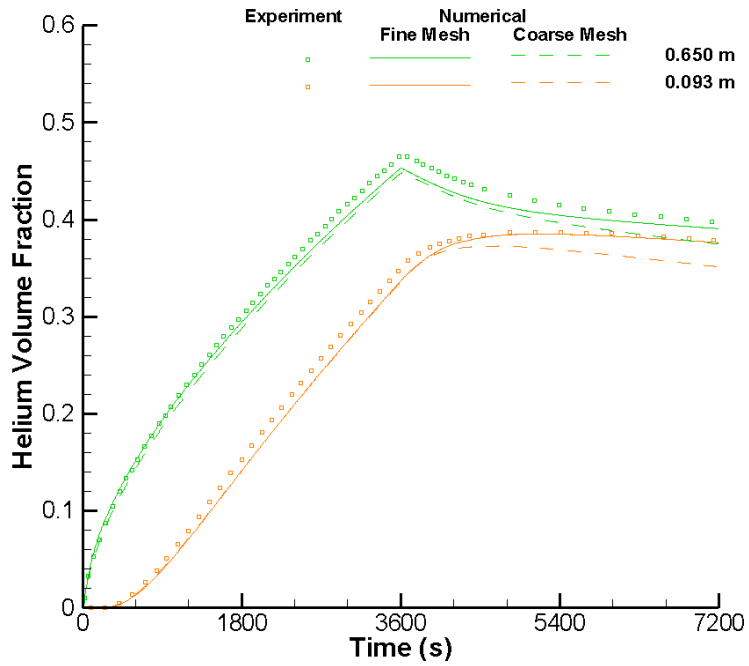


Figure 22. Effect of changing the mesh density in the vertical direction on the predicted helium volume fraction.

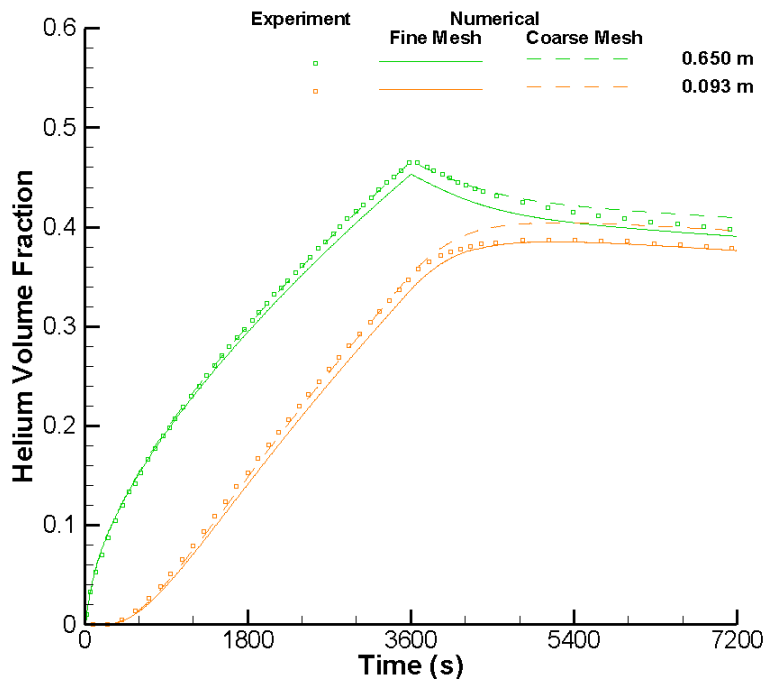


Figure 23. Effect of changing grid density in the horizontal direction on the predicted helium volume fraction.

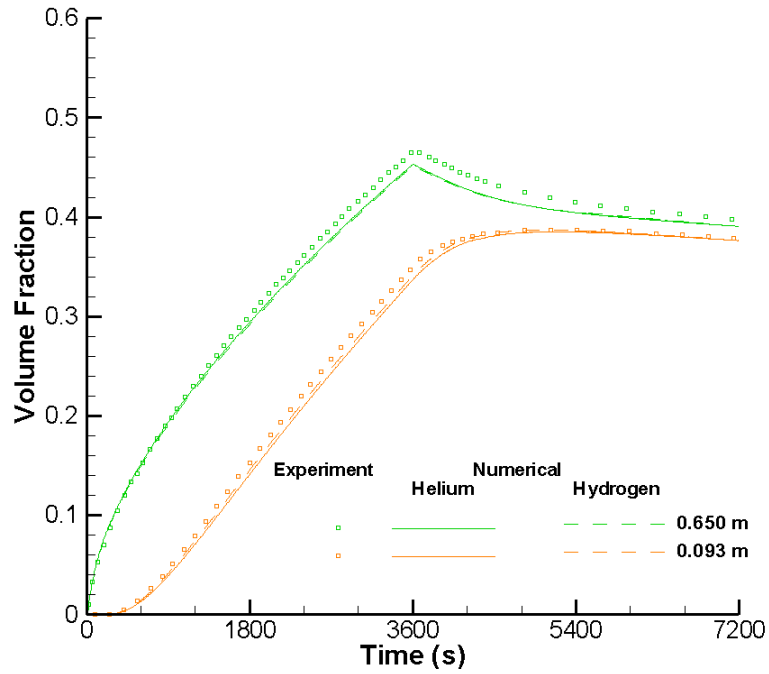


Figure 24. Effect of changing the gas released from helium to hydrogen on the predicted volume fraction. The volume flow rates were kept constant for the two cases.